Carbon 117 (2017) 367–375

Contents lists available at ScienceDirect

Carbon

journal homepage: www.elsevier.com/locate/carbon

Grain size-dependent thermal conductivity of polycrystalline twisted bilayer graphene

Tej B. Limbu [a, b, *], Konstanze R. Hahn [c], Frank Mendoza [a], Satyaprakash Sahoo [d], Joshua James Razink [e], Ram S. Katiyar [a, b], Brad R. Weiner [a, f], Gerardo Morell [a, b]

[a] Institute for Functional Nanomaterials, University of Puerto Rico, San Juan, PR 00931, USA
[b] Department of Physics, University of Puerto Rico at Rio Piedras, San Juan, PR 00931, USA
[c] Department of Physics, University of Cagliari, Cittadella Universitaria, 09042 Monserrato, Italy
[d] Institute of Physics, Bhubaneswar, Odisha, India
[e] Center for Advanced Materials Characterization, University of Oregon, Eugene, OR 97403, USA
[f] Department of Chemistry, University of Puerto Rico at Rio Piedras, San Juan, PR 00931, USA

ARTICLE INFO

Article history:
Received 27 November 2016
Received in revised form
15 February 2017
Accepted 22 February 2017
Available online 3 March 2017

ABSTRACT

We report the room temperature thermal conductivity of polycrystalline twisted bilayer graphene (tBLG) as a function of grain size measured by employing a noncontact optical technique based on micro-Raman spectroscopy. Polycrystalline tBLG sheets of different grain sizes were synthesized on copper by hot filament chemical vapor deposition. The thermal conductivity values are 1305±122, 971±73, and 657±42 $Wm^{-1}K^{-1}$ for polycrystalline tBLG with average grain sizes of 54, 21, and 8 nm, respectively. Based on these thermal conductivity values, we also estimated the grain boundary conductance, $14.43\pm1.21\times10^{10}$ $Wm^{-2}K^{-1}$, and the thermal conductivity for single crystal tBLG, 1510±103 $Wm^{-1}K^{-1}$. Our results show that the relative degradation of thermal conductivity due to grain boundaries is smaller in bilayer than in monolayer graphene. Molecular dynamics simulations indicate that interlayer interactions play an important role in the heat conductivity of polycrystalline bilayer graphene. The quantitative study of the grain size dependent thermal conductivity of polycrystalline bilayer graphene is valuable in technological applications as well as for fundamental scientific understanding.

1. Introduction

Graphene, a single layer of sp^2 bonded carbon atoms, has drawn the attention of the scientific community for many applications due to its excellent electrical, mechanical, optical, and thermal properties [1–6]. Given the high room temperature electron mobility of up to 200000 $cm^2V^{-1}s^{-1}$ for non-suspended monolayer graphene [7], it is a promising material for future ultrafast electronics. Due to the absence of a band gap, graphene's applications are restricted to various electronic devices, such as transistors, which require a high on-off resistance ratio. Bernal stacked bilayer graphene is a potential material for future ultrafast electronics such as transistors and detectors with similar properties to monolayer graphene, but with the additional ability to acquire a tunable band gap under the application of a vertical electric field [7,8]. The graphene bilayer system becomes even more interesting when the two monolayers are rotated relative to each other to produce a twisted bilayer graphene (tBLG). The tunable interlayer coupling and band structure, and the emergence of van Hove singularities in the density of states due to the overlapping of the Dirac cones from top and bottom graphene layers in tBLG, show great potential for future electronic and optoelectronic devices [9,10].

Although ultrafast nanoscale devices can be produced, the generation of heat in the device components from the electric current imposes a challenge to operating performance and device lifetime. Heat management in a device is effective if the integrated materials are capable of transporting the heat to the sink or surroundings, i.e., high thermal conductivity (K) is required. Since the thermal conductivity of bilayer graphene is known to be high, ranging from (1412.8–2800 $Wm^{-1}K^{-1}$), [11,12] it may be a suitable candidate material for ultrafast nano-electronics with an ability of

* Corresponding author. Department of Physics, University of Puerto Rico, San Juan, PR 00931, USA.
E-mail address: tejnembang@yahoo.com (T.B. Limbu).

http://dx.doi.org/10.1016/j.carbon.2017.02.066

heat dissipation.

At present, the most common and scalable technique to synthesize large area polycrystalline graphene is chemical vapor deposition of methane on copper substrates [5,6,13–15]. Grain boundaries are known to scatter phonons and introduce mode mismatch that degrades the thermal conductivity of polycrystalline graphene [16–23]. Several theoretical studies [16–21] have been performed on the thermal transport properties of polycrystalline graphene and grain boundary effects where thermal conductivity is found to decrease with a reduction in graphene grain size. The thermal conductivity of graphene is sensitive not only to grain boundaries but also to defects [24,25], such as point defects and Stone-Wales defects. By using non-equilibrium molecular dynamics simulations, Zhang et al. [24] demonstrated that the thermal conductivity of monolayer graphene decreases rapidly in the small defect density regime of monovacancy, divacancy, and Stone-Wales defects. In the large defect density regime, the thermal conductivity decreases more slowly. In order to use graphene for thermal management applications, the degradation of its thermal conductivity by grain boundaries and defects needs to be understood. Besides the use of its high thermal conductivity for heat dissipation in nanoscale devices, graphene with low thermal conductivity can be utilized for thermoelectric energy conversion [26]. Therefore, the ability to tune the thermal conductivity of graphene by controlling the amount of defects, functionalization, hydrogenation, and grain boundaries [26] is technologically important.

Since graphene is more readily available in polycrystalline form when it comes to obtaining large areas, understanding the physical properties of polycrystalline graphene is critically important for its practical applications. In this context, we hereby report a detailed experimental investigation on the room temperature thermal conductivity of polycrystalline twisted bilayer graphene (tBLG) as a function of grain size. The investigation on the grain size dependent thermal conductivity of tBLG provides information to assess the suitability of this material for future applications in optoelectronics and other nanoscale electronic devices.

2. Experimental details

2.1. Graphene growth by hot filament chemical vapor deposition

Twisted bilayer graphene samples were grown on copper foil (Alfa-Aesar, 0.025 mm thick, annealed, uncoated, 99.8%, metal basis) in a hot filament chemical vapor deposition (HFCVD) reactor by using methane gas as the carbon precursor gas. We synthesized nanocrystalline tBLG of different grain sizes by flowing 10, 5, and 2 sccm of methane gas along with 50 sccm of hydrogen into the chamber for 30 min while the substrate heater temperature was kept at 975 °C. The filament temperature and the total chamber pressure were maintained at 1750 °C and 35 Torr respectively.

2.2. Graphene transfer onto grid

We transferred the graphene from copper foil to the bare copper grid (without holey amorphous carbon) containing circular holes (about 6.5 μm diameter) by a polymer free transfer method. Graphene transfer by using poly(methyl methacrylate) (PMMA) leaves some contamination on graphene which suppresses the phonon transport [27]. Since our bare copper grid does not contain a holey amorphous carbon layer and the grid is much thicker than the usual holey amorphous carbon transmission electron microscopy (TEM) grids, the direct transfer of graphene onto the TEM grid as proposed by Regan et al. [28] was not suitable. We employed a different polymer free transfer method to transfer our bilayer graphene onto the bare copper grids. The tBLG/Cu without any polymer support was directly placed in 20% ammonium persulfate solution in a petri dish for about 2 h (Fig. 1a). Following completion of the Cu etching, the floating bilayer graphene on transparent ammonium persulfate is visible to the naked eye (better with a simple hand lens). This method is suitable specifically for bilayer and multilayer graphene due to their higher opacity compared to monolayer graphene. We placed a clean white sheet of paper under the petri dish to help us see the floating graphene from directly above. The floating graphene was then picked with a glass plate (Fig. 1b) and transferred to deionized (DI) water in a glass beaker for further cleaning (Fig. 1c). A white paper was also placed under the beaker. After 30 min, the graphene was transferred onto DI water and the process was repeated four times. Finally, the clean graphene was scooped with a Cu grid (Fig. 1d), and dried on a hot plate at 45 °C for 5 min.

2.3. Characterization of graphene

The synthesized graphene samples were characterized by using Raman spectroscopy (Horiba-Jobin T64000 micro-Raman system equipped with a diode laser emitting at 514.5 nm), scanning electron microscopy (SEM, JEOL JSM-7500F), spherical aberration-

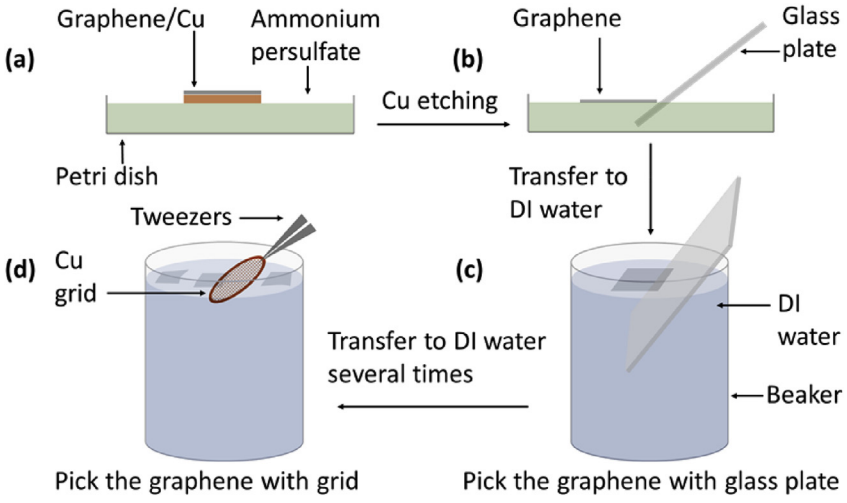

Fig. 1. Schematic illustration of the transfer process employed for bilayer graphene.

corrected high-resolution transmission electron microscope (HRTEM) (Titan), and atomic force microscopy (AFM) (Nanoscope V (Vecco)) equipped with a silicon nitride tip with back side coating (Ti/Au 45 nm).

2.4. Experimental measurement of thermal conductivity

We measured the thermal conductivity of suspended polycrystalline bilayer graphene by employing a non-contact Raman optothermal technique [1,2,11,25]. This is a non-invasive technique, and is suitable to apply when a material is in suspended form. Thermal conductivity extraction from suspended graphene avoids the effect of strains [2] and graphene-substrate interactions [15], which allows us for a direct comparison on the phonon transport properties of polycrystalline bilayer graphene of different grain sizes. The graphene was suspended over a relatively large grid hole (~6.5 μm) compared to the laser spot size of ~1.5 μm. The Raman peak position was calibrated and monitored using the 521.7 cm^{-1} peak of silicon every 2 h during the measurements. The Raman spectra were further improved by sufficiently long acquisition of 2 min. The frequency shift of one of the intense Raman bands (i.e., the G peak in our case) is analyzed separately as a function of the temperature of the material and absorbed laser power. The thermal conductivity measurement process is divided into two steps: a calibration procedure and the power-dependent Raman measurement.

In our calibration experiments, we recorded the Raman G peak position as a function of temperature. The samples were placed in a cold-hot cell (Enkam TS1500) temperature controller. The spectra were recorded at temperature intervals of 25 K ranging from 83 to 473 K. For each Raman measurement, the samples were kept at the intended temperature for 5 min in order to allow for temperature stabilization. The calibration Raman measurements were performed at a low laser excitation power of ~ 0.5 mW to minimize local heating by the laser radiation.

The laser power dependent Raman measurements were carried out at room temperature in air with the laser beam at the center of the graphene suspended over the grid hole. The laser radiation produced local heating at the center of the suspended graphene and the Raman spectrum was collected for 2 min. Due to the negligibly small thermal conductivity (~0.025 W/mK) of air [1], we assume that the local heat developed at the laser spot only propagates along the plane of graphene. We measured the power absorbed by the suspended graphene by using a laser power meter (FieldMaster) equipped with a semiconductor laser sensor (Coherent, model LM-2). The measurement of the absorbed power by the suspended graphene was performed after all of the power dependent Raman measurements were carried out. We measured the power transmitted through an empty hole and that transmitted through the graphene layer, the difference of which gives the power absorbed by the suspended graphene. The small radiation reflectivity (0.1%) [15] of graphene was disregarded. The experiments were repeated on three regions of the suspended graphene and they were reproducible within 10%.

2.5. Thermal conductivity calculation by molecular dynamics simulations

The thermal conductivity of the monolayer and twisted bilayer graphene has been calculated by MD simulations. MD simulations have been performed using the large-scale atomic/molecular massively parallel simulator (LAMMPS) code [29,30] and covalent interactions between carbon atoms have been described by the second-generation reactive empirical bond order (REBO) potential. The REBO potential has been shown previously to describe reasonably well the C–C bonds in single crystalline and polycrystalline monolayer graphene [17,31–33]. It does not explicitly consider long-range dispersion interactions. Therefore, a Lennard-Jones potential has been added to account for such a dispersion interaction between the layers of bilayer graphene.

The thermal conductivity has been calculated based on an approach to equilibrium molecular dynamics (AEMD) methodology. Details on the AEMD procedure can be found elsewhere [34,35]. Simulation cells of nanocrystalline graphene have been generated using an iterative algorithm as described previously [17]. We calculated the thermal conductivity of nanocrystalline tBLG of mixed arbitrary twist angles with grain sizes ranging from 5.0 to 22.5 nm at the simulation cell length (L) of 200 nm. For comparison, we calculated the thermal conductivity of nanocrystalline monolayer graphene of grain sizes ranging from 1.3 to 41.4 nm at the same simulation cell length. The thermal conductivity of the corresponding single crystalline system (K_C) at the same simulation cell length (200 nm) has been determined from the $1/K$ to $1/L$ behavior [17], where K is the thermal conductivity of a nanocrystalline graphene at a simulation cell length of L.

3. Results and discussion

3.1. Graphene growth and characterization

We synthesized tBLG of different grain sizes on copper foil by HFCVD. Although graphene growth on copper in the HFCVD is similar to the growth in thermal CVD, a distinct feature of the HFCVD growth is that a fraction of the methane and hydrogen gases are decomposed at the hot filaments prior to interacting with the hot copper surface, which favors the formation of a second layer, leading to the growth of bilayer graphene islands. The islands continue to grow with deposition time and finally merge to form a large area polycrystalline bilayer graphene. It is known that graphene grows on copper by carbon nucleation on the copper surface which grows with time into graphene grains [36,37]. Hence, by controlling the carbon nucleation density, bilayer graphene of variable grain sizes can be grown.

The nanocrystalline nature of the synthesized graphene samples was confirmed based on the Raman spectroscopic characterization and TEM studies. Raman spectra of all nanocrystalline tBLG samples on bare copper TEM grids having different defect densities are shown in Fig. 2. They show the characteristic Raman G and 2D

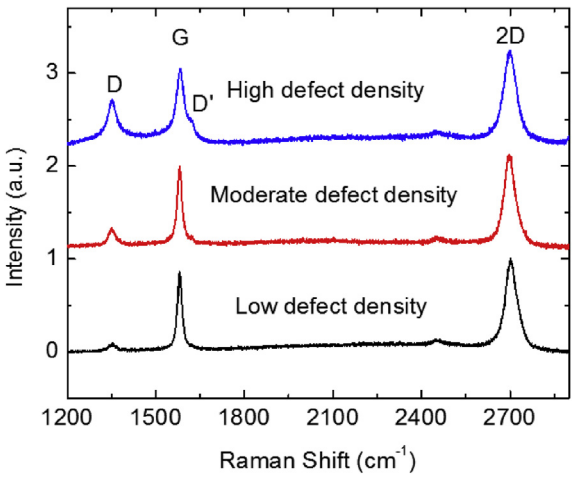

Fig. 2. Raman spectra of tBLG materials: black color for low defect density, red for moderate defect density, and blue for high defect density. (A colour version of this figure can be viewed online.)

bands at around 1582 and 2696 cm^{-1}, respectively, with a slight tendency of the more defective graphene to have a lower G mode frequency. The D and D′ bands, which are activated by single phonon intervalley and intravalley scattering processes [38], appear at 1350 and 1621 cm^{-1}, respectively.

It is evident from the tBLG Raman spectra that the D and D′ bands are small, the D′ band is distinguishable from the G band as a shoulder, and the G bands are narrow. These Raman features indicate that the defects in the graphene fall in the first category as classified by Ferrari and Robertson [39]. For this category of defects, the Tuinstra and Koenig relation [40],

$$I(D)/I(G) = C(\lambda)/d \quad (1)$$

can be applied to estimate the grain size (d) in the graphene, where the co-efficient $C(\lambda)$ is ~4.4 nm [40] for laser excitation wavelength, $\lambda = 514.5\ nm$. Ten different Raman spectra were collected at room temperature for each sample from the suspended region of graphene by probing the laser beam on the studied grid hole and the surrounding holes. The intensity ratio ($I(D)/I(G)$) of the D and G bands was obtained by fitting the bands to the damped harmonic oscillator function (phonon model) (see Fig. S1 in the supplementary material section). The average grain sizes, estimated by using equation (1), for the tBLG with high, intermediate, and low defect density, are 8.0±1.1, 21.2±2.5, and 53.9±6.6 nm, respectively. The standard deviation (σ) was taken as the error for the estimated grain size.

Fig. 3a shows the representative tapping mode AFM image of the tBLG lying flat on SiO_2/Si. The measured height profile (inset) of the tBLG is 1.1 nm, which indicates that the graphene consists of two layers [5]. Fig. 3b is the representative field emission SEM image of the suspended nanocrystalline tBLGs on the bare copper grid transferred by our method where graphene is lying flat on the surface of the copper grid, well stretched over the holes, with a few acquired wrinkles. Representative HRTEM images of nanocrystalline tBLG are shown in Fig. 3c and d. They show a Moiré pattern due to the two layers rotated relative to each other by an angle. The fast Fourier transform of the images in Fig. 3c and d (insets) shows two sets of six-fold reflection spots rotated to each other by an angle indicating that the graphene is a tBLG. The statistical analysis indicates that the dominant twist angle is ~21°.

3.2. Temperature-dependent Raman studies

Fig. 4a shows the dependence of the G peak spectral position on temperature for nanocrystalline tBLG with different grain sizes. The Raman spectra as a function of temperature for an average grain size of 54 nm is shown in the Supplementary Material section (Fig. S2). The G peak red-shifts linearly with the increase in temperature from 83 to 473 K for all the grain sizes, which is attributed to a combined effect of volume and temperature contributions, resulting from the anharmonicity in the lattice [41]. We found the red-shifted values to be consistently reproducible within 10%. The effect of strain on the G peak shift in the suspended graphene has been reported to be small compared to that of temperature [15]. Also, since our graphene layers have been transferred by polymer free method, there is no G peak shift caused by the possible charge transfer doping from its residues, and any doping by atmospheric molecules is uniform. Taking into account the uncertainty in the G peak position (Fig. 4a) at any particular temperature, the measured values overlap at most of the temperatures for the three grain sizes studied. Also, the individually calculated slopes completely overlap

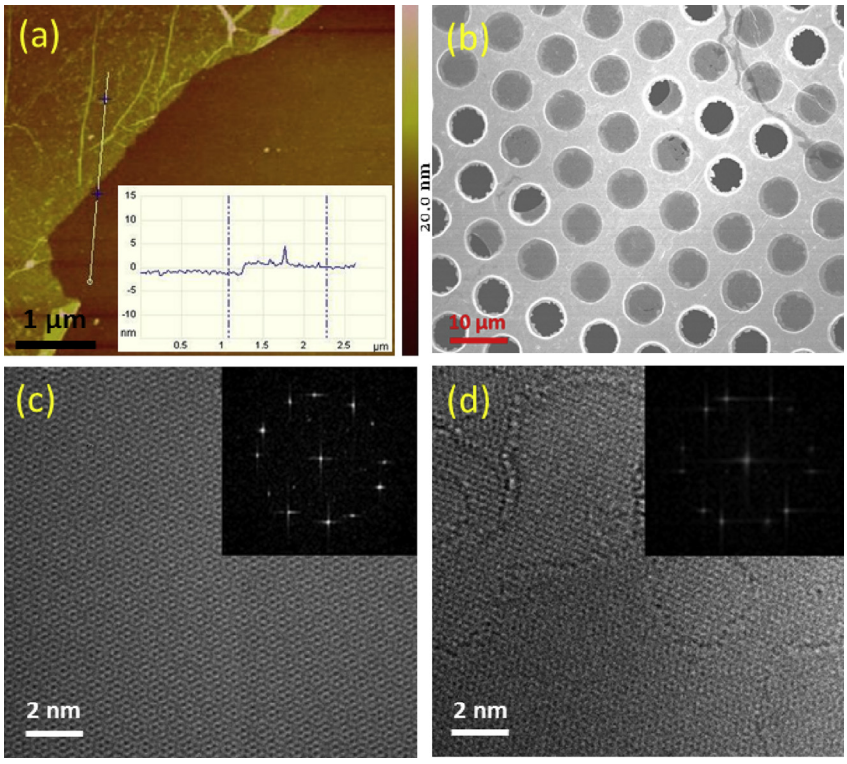

Fig. 3. (a) Tapping mode AFM image of bilayer graphene on SiO_2/Si. Inset shows the height profile of the graphene film along the white line, showing a step height of 1.1 nm; (b) Field emission SEM image of suspended nanocrystalline tBLGs on bare copper grid; (c) Representative HRTEM image of nanocrystalline tBLG for grain sizes of ~21 and ~54 nm showing a Moiré pattern; (d) Representative HRTEM image of nanocrystalline tBLG for a grain size of ~8 nm showing a Moiré pattern in each grain. Insets are the FFT of the images, showing two sets of six-fold reflection spots corresponding to the two graphene monolayers of the bilayer system rotated with respect to each other with a twist angle of ~21°. (A colour version of this figure can be viewed online.)

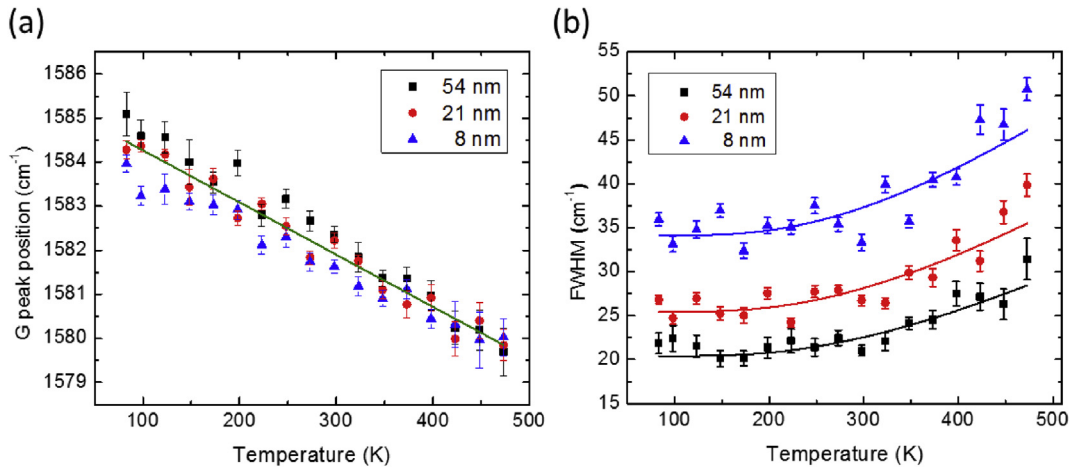

Fig. 4. (a) A single linear plot of Raman G peak position vs temperature for suspended tBLG with different grain sizes. The experiments were performed at ~ 0.5 mW of laser power. (b) Decay rate of the G-mode optical phonons in nanocrystalline tBLG with different grain sizes. The experimental data (symbols) are fit (thick solid lines) to Equation (2).

due to this uncertainty. Hence, there is no significant difference in the measured values of the temperature dependence of the G peak position shift for different grain sizes. We fitted a single line to the data by considering the following linear equation $\omega = \omega_0 + \alpha T$, where ω_0 is the phonon frequency at 0 K, and α is the first order temperature coefficient. The fitted temperature co-efficient α is $-(1.20\pm0.06) \times 10^{-2}\ cm^{-1}K^{-1}$ which is slightly smaller than the previously reported values for bilayer graphene [11,41].

We analyzed the temperature dependence of the G-mode phonon decay rates of the suspended nanocrystalline tBLG with different grain sizes. We did not observe significant temperature dependence below room temperature for all the grain sizes, whereas the phonon decay rate increases gradually beyond that temperature. Chatzakis et al. [42] reported a similar observation for the temperature dependence of the G-mode optical phonon decay rate for highly oriented pyrolytic graphite (HOPG) and single walled carbon nanotubes (SWCNTs). The G-mode phonon decay process can be explained by the decay of this zone center optical phonon mode (G-mode) into two phonons of smaller energy governed by the following equation [42];

$$\Gamma(T) = \Gamma_0 + A\,[1 + n(\omega_1, T) + n(\omega_2, T)] \quad (2)$$

where $\Gamma(T)$ is the temperature dependent phonon line width or full width at half maximum (FWHM), Γ_0 is the linewidth at zero temperature, A is the anharmonic coefficient, $n(\omega, T)$ is the Bose–Einstein distribution function, and ω_1 and ω_2 are the frequencies of the daughter phonons into which the G-mode phonon decays. The experimental data for all the nanocrystalline tBLG with different grain sizes can be fit to equation (2) (Fig. 4b) using two optical phonons with frequencies 896.36 and 688.10 cm^{-1} at Γ point reported elsewhere [43] for a twisted bilayer graphene of twist angle 21.8°. We note that these two optical phonons are also commonly present in twisted bilayer graphene of other twist angles 13.2°, 9.4°, and 7.3° [43] which forms a portion of our nanocrystalline twisted bilayer graphene. These two phonon energies correspond to the maximum (DOS) region for the tBLG of 21.8° and 13.2° [43] and nanocrystalline monolayer graphene [16,17]. The values of the fitting parameters Γ_0 and A are presented in Table 1, which shows that the values of Γ_0 increase with the decrease.in the grain size indicating that the lifetime of G-mode phonon is shorter for smaller grain size graphene. Furthermore, the value of A is found to be increasing with the decrease in the grain size which can be explained as the enhancement of the anharmonic interaction by the grain boundaries in smaller grained graphene. The increase in the G-mode phonon decay rate ($\Delta\Gamma$) in the studied temperature range (83–473 K) is larger for smaller grain sizes. This value (see Table 1) increases from 1.5 to 2.3 ps^{-1} as the grain size decreases from 54 to 8 nm. We observed a relatively fast increase in the phonon decay rate in our nanocrystalline twisted bilayer graphene over the studied temperature range with respect to HOPG and SWCNT [42]. This can be explained by the numerous folded low energy phonon modes inherently produced in twisted bilayer graphene [11,43] due to the Brillouin zone folding and the presence of phonon DOS for such a low energy. The daughter phonons with energy 896.36 and 688.10 cm^{-1} [43] produced from the decay of the G-mode phonon are likely to decay into such low energy phonons. The low energy phonons can be activated by heat as their energy is comparable to the thermal energy in the studied temperature range. Overall, the presence and activation of numerous folded low energy phonons in twisted bilayer graphene and the grain boundaries in the nanocrystalline graphene enhance the scattering and decay of the G-mode phonon leading to its faster decay when the temperature is increased above room temperature.

3.3. Laser power dependent Raman studies and thermal conductivity measurement

For the laser power dependent Raman measurements, we placed the graphene/grid on a silicon substrate positioned at an incline angle of 45° to the sample holder and the grid, as shown in Fig. 5a, to avoid the multiple power absorption by graphene. A portion of the incident laser energy at the center of the suspended graphene is absorbed. The measured optical absorption at 514.5 nm is 7.5±0.7%, which is comparable to the literature values for bilayer graphene [11]. The heat produced at the center of the suspended graphene propagates along the graphene sheet, and radially outwards to the edges of the grid hole. The copper grid helps to dissipate the heat as copper is a good thermal conductor ($\approx$400 Wm^{-1}K^{-1} at room temperature) [44]. The heat developed at the center of the suspended graphene raises the local temperature causing the red shift of the Raman G peak. Hence, it is expected that the red shift of Raman G peak increases with the increase in the laser power. Fig. 5b shows the plots of the Raman G peak position vs absorbed laser power for different nanocrystalline tBLG. The slopes give the values of the change in G-mode phonon frequency with

Table 1
The values of the fit parameters and phonon decay rates using Equation (2) to describe the experimental temperature dependence of the anharmonic decay rate of the G-mode phonons for nanocrystalline tBLG of different grain sizes.

Grain size (nm)	Γ_0 (cm^{-1})	A (cm^{-1})	Γ (cm^{-1}) at 83 K	Γ (cm^{-1}) at 473 K	$\Delta\Gamma$ (cm^{-1})	$\Delta\Gamma$ (ps^{-1})
8.0±1.1	27.7±1.7	6.5±1.1	34.0±2.1	46.1±2.8	12.1±3.5	2.3±0.6
21.2±2.5	20.0±1.3	5.4±0.9	25.5±1.7	35.5±2.3	10.0±2.9	1.9±0.6
53.9±6.6	16.1±0.9	4.3±0.6	20.4±1.2	28.4±1.6	8.0±2.0	1.5±0.4

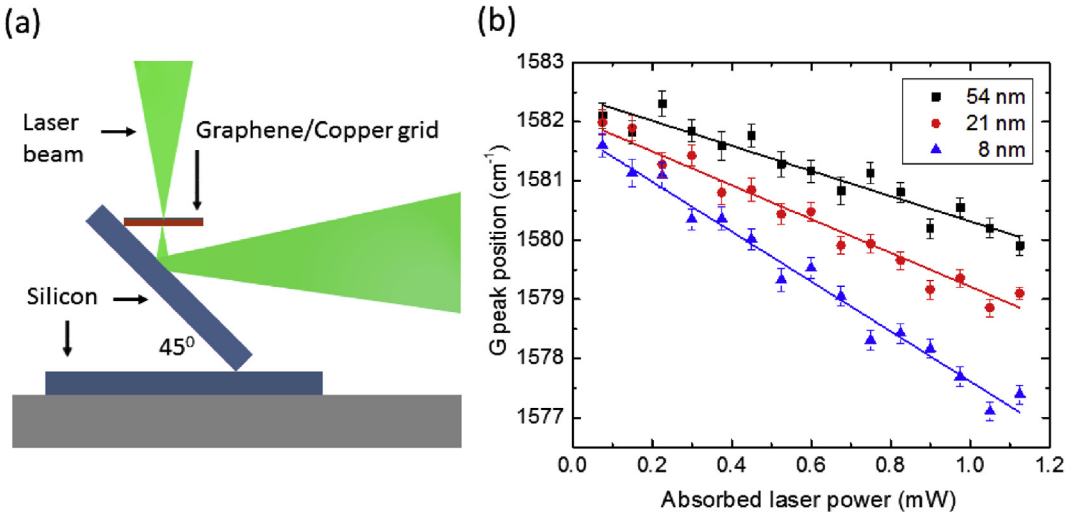

Fig. 5. (a) A schematic diagram of laser probing on graphene/Cu grid for laser power-dependent Raman measurement. (b) Plots for the G peak shift vs absorbed laser power for different grain sizes. The data are fitted with black (54 nm average grain size), red (21 nm average grain size), and blue (8 nm average grain size) lines.

incident laser energy $(\delta\omega/\delta P)$. The obtained values of $(\delta\omega/\delta P)$ are −2.12±0.17, −2.86±0.16, and −4.21±0.18 cm^{-1}/mW for the tBLG of average grain sizes 54, 21, and 8 nm, respectively. The smaller value of $(\delta\omega/\delta P)$ for larger grained graphene indicates that heat is dissipated more efficiently by such graphene.

The expression for the thermal conductivity in the radial heat wave case proposed by Balandin et al. [1] is given by equation (3):

$$K = \alpha \left(\frac{1}{2\pi h}\right)\left(\frac{\delta\omega}{\delta P}\right)^{-1} \quad (3)$$

where h is the thickness of bilayer graphene in our case. The values of K for tBLG with average grain size of 54, 21, and 8 nm are: 1305±122, 971±73, and 657±42 $Wm^{-1}K^{-1}$ respectively. Since the graphene/grid was kept at ambient temperature during the laser power dependent Raman measurements, the measured thermal conductivity values correspond to room temperature. Nonetheless, it has been widely studied [2,11,15,49] that irrespective of the number of layers, the thermal conductivity of graphene decreases with increase in temperature above room temperature.

The experimental uncertainties on the measured room temperature thermal conductivity values of the nanocrystalline tBLG include random uncertainties of the measured temperature coefficient, laser power dependent Raman studies, and measurement on the laser power absorption. We have taken care of several factors to minimize the possible random uncertainties on the measurements such as temperature stabilization for 5 min for every subsequent temperature measurement Raman studies, sufficiently long Raman spectrum acquisition (2 min), and cleanliness of the samples. Possible systematic uncertainty on the Raman peak position has been controlled by calibrating and monitoring the peak position using 521.7 cm^{-1} peak of silicon every 2 h during the Raman measurements.

The tBLG with average grain size 54 nm has a relatively small defect density introduced by the grain boundaries, and hence its K value is comparable to 1413 ± 390 $Wm^{-1}K^{-1}$ for CVD synthesized twisted bilayer graphene with a twist angle of 34° with negligible defects reported by Li et al. [11]. Since the twist angle between the graphene monolayers influences the phonon spectra of the tBLG by modification of the weak van der Waals inter-layer interaction, and alteration of the size of the Brillouin zone leading to the phonon momentum change [43], the thermal conductivity of a twisted bilayer graphene is dependent upon the twist angle (θ). The direct comparison of the thermal conductivity values for different tBLG with different twist angle is therefore not appropriate. We note that the intrinsic thermal conductivity of a tBLG is lower relative to that of AB stacked bilayer graphene [11]. In a twisted bilayer graphene, two atomic planes are coupled weakly by van der Waals interactions but phonons do not propagate as in two nearly independent SLG planes [11]. The twist between the atomic planes in tBLG results in the substantially reduced size of the Brillouin zone and the emergence of numerous folded acoustic phonon branches, which facilitate the momentum conservation for normal three phonon scattering.

3.4. Estimation of grain boundary conductance

We found that thermal conductivity of polycrystalline bilayer graphene decreases with the reduction in grain size, and it decreases faster in the small grain regime (see Fig. S3 in the Supplementary Material section), consistent with theoretical results [17,19,22]. Considering that the heat flux is perpendicular to the grain boundaries, the thermal conductivity in nanocrystalline graphene can be described as a connection of resistances in series. The

total phonon thermal conductivity (K) of polycrystalline graphene is expressed in terms of the boundary conductance (G) of the grain boundaries, the magnitude of the grain size (d), and the thermal conductivity (K_g) of the grain regions as [17–19,22,33]:

$$\frac{1}{K} = \frac{1}{G\,d} + \frac{1}{K_g} \tag{4}$$

Equation (4) shows that the plot of the inverse of thermal conductivity, K, versus the inverse of the grain size, d, is a linear curve, the slope of which gives the value of boundary conductance, and the y-intercept gives the value of the thermal conductivity $K_p (K_g = K_p$ for infinitely large grain) of the infinitely large grain (single crystalline graphene). Fig. 6 shows a linear fit of the plot of $1/K$ versus $1/d$ yielding the values of $14.43\pm1.21 \times 10^{10}\ Wm^{-2}K^{-1}$ and $1510\pm103\ Wm^{-1}K^{-1}$ for the thermal boundary conductance and thermal conductivity of the single crystalline tBLG, respectively. The obtained value of grain boundary conductance is 3–10 times larger than the calculated values in the previous reports [17,18,22,45,46], but close to the value $13.3 \times 10^{10}\ Wm^{-2}K^{-1}$ estimated by Reference [19] for monolayer graphene.

The extrapolated value of thermal conductivity of tBLG is reasonable with respect to the literature values for the suspended bilayer graphene [11,47], and reported theoretical values [48,49]. The value is slightly larger than the experimentally measured value of tBLG of twist angle 34° (equivalent to 4°) [11], but is consistent if we consider that our graphene is a twisted bilayer graphene of 21°. tBLG of twist angle 21.8° has the smallest sized Moiré supercell (unit cell) with a commensurate atomic configuration. The twist angle in a tBLG with commensurate atomic configuration is given by Ref. [43]:

$$\cos(\theta) = \frac{(3m^2 + 3mn + m^2/2)}{(3m^2 + 3mn + 3n^2)} \tag{5}$$

where m and n are the positive integers.

If n is not divisible by 3, the number of atoms in the unit cell of tBLG for a given pair of integers (m, n) is given by:

$$N = 4\left[(m+n)^2 + m(2m+n)\right] \tag{6}$$

The prevailing twist angle in our tBLG is ~21°, close to the theoretical value of 21.8° for a commensurate atomic configuration. For such a case, the values of (m, n) are $(1, 1)$, which gives the number of the C atoms in the unit cell as 28. Hence, there are roughly a total of 84 possible phonon branches in the phonon spectrum of the tBLG of twist angle ~21°. This number is larger than 6 for single layer, 12 for AB or AA stacked bilayer graphene, but substantially smaller than that of a tBLG of any twist angle. Based on the fact that the Brillouin zone of the tBLG with a twist angle of 21.8° is the largest among the tBLG of all possible twist angles, Umklapp phonon scattering is expected to be minimal for this twist angle. Since there are a minimum number of folded phonon branches in 21° twisted bilayer graphene compared to those of other twist angles, phonon momentum conservation for normal scattering is also minimized [11]. Hence, we can expect the phonon thermal conductivity in tBLG of ~21° is greater than the tBLGs of other twist angles.

3.5. MD simulations and comparison of normalized thermal conductivity

Looking into the relative change in thermal conductivity for nanocrystalline tBLG as a function of grain size, the values decrease to 86%, 64%, and 43% (taking $K_P = 1510\ Wm^{-1}K^{-1}$ as the reference value) for 54, 21, and 8 nm average grain sizes, respectively. By comparing these values with those reported for monolayer graphene with similar grain sizes [16,17,19], we find that the relative decrease in the thermal conductivity of nanocrystalline tBLG is smaller than that of monolayer graphene. For example, the thermal conductivity is reduced to about 25% for 8-nm grain size polycrystalline monolayer graphene [19], in contrast to 43% for 8-nm grain size tBLG. In order to understand this result, we performed MD simulations to obtain the normalized thermal conductivity (K/K_{ref}) for nanocrystalline tBLG as a function of grain size. For comparison, we performed a similar calculation for monolayer graphene. Details of the nanocrystalline graphene sheet constructed for the simulations (see Fig. S4) are provided in the Supplementary Material section.

Fig. 7 compares the K/K_{ref} vs d behavior of the experimental data for nanocrystalline tBLG, with the data from simulations for nanocrystalline tBLG and monolayer graphene. It is evident from Fig. 7 that the K/K_{ref} vs d behavior for the tBLG from experimental results resembles that of the tBLG of the simulation results. The

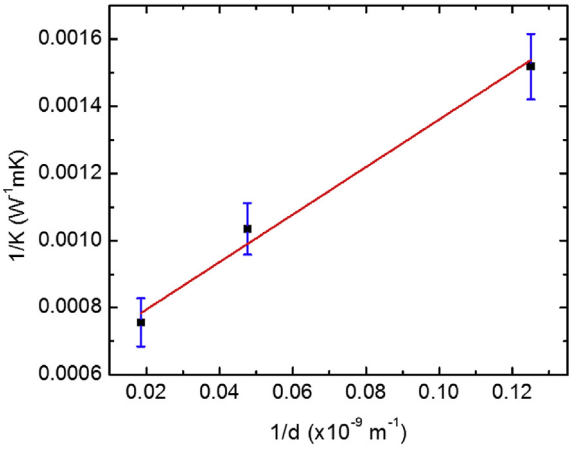

Fig. 6. Inverse of thermal conductivity versus the inverse of grain size (d). Red line is the linear fit, the slope of which gives the value of boundary conductance, $14.43\pm1.21 \times 10^{10}\ Wm^{-2}K^{-1}$, and the y-intercept gives the value of the thermal conductivity for single crystalline tBLG, $1510\pm103\ Wm^{-1}K^{-1}$. (A colour version of this figure can be viewed online.)

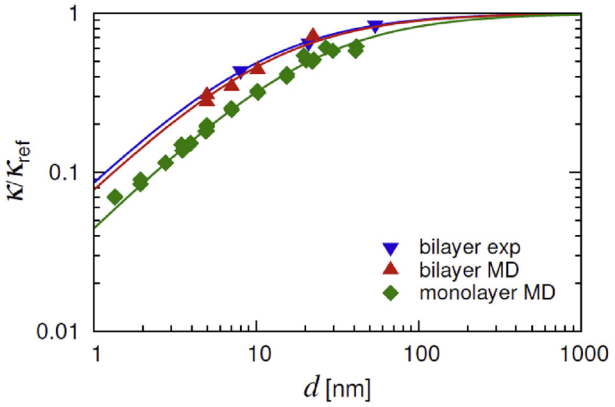

Fig. 7. Normalized thermal conductivity K/K_{ref} as a function of grain size (d). The thermal conductivity of the HFCVD grown nanocrystalline tBLG (blue filled inverted triangles) have been normalized to $K_{ref} = K_P$. The thermal conductivity for monolayer (green filled diamonds) and twisted bilayer (red filled triangles) graphene obtained from MD simulations have been normalized to the corresponding values of K_{ref}. (A colour version of this figure can be viewed online.)

extrapolated curve for the experimental result shows that at a grain size of 1 nm, the thermal conductivity of the tBLG is reduced to about 9% of the thermal conductivity corresponding to a single crystalline system. This is close to the simulation results for the tBLG, where the thermal conductivity is reduced to about 8% at a grain size of 1 nm. The simulation results shows that the grain boundary effect on the degradation of thermal conductivity for a monolayer graphene is significantly larger than in a bilayer graphene. The thermal conductivity of a nanocrystalline monolayer graphene is reduced to about 4% when the grain size is 1 nm, consistent with the reports [17,19].

A smaller degradation to the thermal conductivity due to grain boundaries is observed in polycrystalline bilayer graphene versus that in monolayer graphene. This may be explained as follows: many reports [1,4,15,47–51] claim that the out of plane acoustic (ZA) (flexural) phonons dominate the in-plane acoustic (Longitudinal/Transverse) phonons for thermal conductivity in graphene. In the bilayer system, the two graphene planes are coupled through a weak van der Waals interaction [47]. Such an interplanar interaction opens many new phonon scattering channels in bilayer graphene, including the most effective one which involves three ZA phonons [49]. In monolayer graphene, these additional scattering channels for flexural phonons are absent. This explains the decrease in the thermal conductivity from monolayer to bilayer graphene [49,51]. In the case of polycrystalline bilayer graphene, grain boundaries in the two interacting graphene layers tend to decouple them, thus, the scattering channels for flexural phonons are reduced enhancing slightly the phonon transport. Such an effect of decoupling the graphene layers in a bilayer system by grain boundaries increases with decreasing grain size due to the increased density of grain boundaries. Hence, we observe similar K/K_{ref} vs d behavior for BLG and monolayer graphene in the large grain regime, and gradual deviation of the curve for BLG (going higher) from the monolayer with reduction in grain size.

4. Conclusions

We report an experimental investigation of the room temperature thermal conductivity of a twisted bilayer graphene as a function of grain size by employing a noncontact technique based on micro-Raman spectroscopy. We synthesized nanocrystalline tBLG with different grain sizes by hot filament chemical vapor deposition using methane as the carbon precursor gas. The bilayer graphene on copper was successfully transferred onto bare copper grids of hole diameter ~6.5 μm. The results show that the thermal conductivity of tBLG is quite high, comparable to that of Bernal bilayer graphene. We estimated the values of thermal boundary conductance and thermal conductivity of the single crystalline tBLG. We also found that the degradation in thermal conductivity due to grain boundaries is smaller in a polycrystalline bilayer graphene than in a polycrystalline monolayer graphene. This result has been understood through MD simulations as resulting from non-negligible interactions between adjacent layers. Our study encourages the grain boundary engineering of CVD synthesized graphene for tuning thermal conductivity for practical applications.

Acknowledgements

This project was partially supported by the Institute for Functional Nanomaterials (NSF Grant 1002410) and PR NASA EPSCoR (NASA Cooperative Agreement NNX15AK43A). The authors thank Prof. Luciano Colombo for providing constructive comments on the manuscript, and Mr. William Pérez for valuable assistance in Raman spectroscopy.

Appendix A. Supplementary data

Supplementary data related to this article can be found at http://dx.doi.org/10.1016/j.carbon.2017.02.066.

References

[1] A.A. Balandin, S. Ghosh, W. Bao, I. Calizo, D. Teweldebrhan, F. Miao, et al., Superior thermal conductivity of single-layer graphene, Nano Lett. 3 (2008) 902–907.
[2] J.-U. Lee, D. Yoon, H. Kim, S.W. Lee, H. Cheong, Thermal conductivity of suspended pristine graphene measured by Raman spectroscopy, Phys. Rev. B 83 (2011) 081419–081423.
[3] A. Rajabpour, S.M. Vaez Allaei, Tuning thermal conductivity of bilayer graphene by inter-layer sp^3 bonding: a molecular dynamics study, Appl. Phys. Lett. 101 (2012) 053115–053119.
[4] Y. Wang, A.K. Vallabhaneni, B. Qiu, X. Ruan, Two-dimensional thermal transport in graphene: a review of numerical modeling studies, Nanoscale Microscale Thermophys. Eng. 18 (2014) 155–182.
[5] T.B. Limbu, F. Mendoza, D. Barrionuevo, J. Carpena, B. Maruyama, R.S. Katiyar, et al., Study on the optical and electrical properties of tetracyanoethylene doped bilayer graphene stack for transparent conducting electrodes, AIP Adv. 6 (2016) 035319–035329.
[6] F. Mendoza, T.B. Limbu, B.R. Weiner, G. Morell, Large-area bilayer graphene synthesis in the hot filament chemical vapor deposition reactor, Diam. Relat. Mat. 51 (2015) 34–38.
[7] J.A. Leon, E.S. Alves, D.C. Elis, J.C. Brant, T.C. Barbosa, L.M. Malard, et al., Rapid fabrication of bilayer graphene devices using direct laser writing photolithography, J. Vac. Sci. Tech. B 29 (2011) 021204–021211.
[8] F. Schwierz, Graphene transistors, Nat. Nanotechnol. 5 (2010) 487–496.
[9] L. Liao, H. Wang, H. Peng, J. Yin, A.L. Koh, Y. Chen, et al., Van Hove singularity enhanced photochemical reactivity of twisted bilayer graphene, Nano Lett. 15 (2015) 5585–5589.
[10] H. Patel, R.W. Havener, L. Brown, Y. Liang, L. Yang, J. Park, et al., Tunable optical excitations in twisted bilayer graphene form strongly bound excitons, Nano Lett. 15 (2015) 5932–5937.
[11] H. Li, H. Ying, X. Chen, D.L. Nika, A.I. Cocemasov, W. Cai, et al., Thermal conductivity of twisted bilayer graphene, Nanoscale 6 (2014) 13402–13408.
[12] H. Zhan, Y. Zhang, J.M. Bell, Y. Gu, Suppressed thermal conductivity of Bi-layer graphene with vacancy-initiated linkages, J. Phys. Chem. C 119 (2015) 1748–1752.
[13] F. Mendoza, T.B. Limbu, B.R. Weiner, G. Morell, Hot Filament Chemical Vapor Deposition: Enabling the Scalable Synthesis of Bilayer Graphene and Other Carbon Materials, Intech Book: Chemical Vapor Deposition - Recent Advances and Applications in Optical, Solar Cells and Solid State Devices (Chapter 4), 2016, pp. 93–107, http://dx.doi.org/10.5772/63921.
[14] X. Li, W. Cai, J. An, S. Kim, J. Nah, D. Yang, et al., Large-area synthesis of high-quality and uniform graphene films on copper foils, Science 324 (2009) 1312–1314.
[15] W. Cai, A.L. Moore, Y. Zhu, X. Li, S. Chen, L. Shi, et al., Thermal transport in suspended and supported monolayer graphene grown by chemical vapor deposition, Nano Lett. 10 (2010) 1645–1651.
[16] P.H. Wu, S.S. Quek, Z.D. Sha, Z.L. Dong, X.J. Liu, G. Zhang, et al., Thermal transport behavior of polycrystalline graphene: a molecular dynamics study, J. Appl. Phys. 116 (2014) 204303–204309.
[17] K.R. Hahn, C. Melis, L. Colombo, Thermal transport in nanocrystalline graphene investigated by approach-to-equilibrium molecular dynamics simulations, Carbon 96 (2016) 429–438.
[18] Y.I. Jhon, M.S. Jhon, Temperature Dependence of Thermal Conductivity of Polycrystalline Graphene: Thermally Enhanced Kapitza Conductance, 2013 arXiv: 1304.6947v1 [cond-mat.mtrl-sci].
[19] B. Mortazavi, M. Pötschke, G. Cuniberti, Multiscale modeling of thermal conductivity of polycrystalline graphene sheets, Nanoscale 6 (2014) 3344–3352.
[20] Z. Aksamija, I. Knezevic, Lattice thermal transport in large-area polycrystalline graphene, Phys. Rev. B 90 (2014) 035419–035427.
[21] H.K. Liu, Y. Lin, S.N. Luo, Grain boundary energy and grain size dependences of thermal conductivity of polycrystalline graphene, J. Phys. Chem. C 118 (2014) 24797–24802.
[22] A. Bagri, S.-P. Kim, R.S. Ruoff, V.B. Shenoy, Thermal transport across twin grain boundaries in polycrystalline graphene from nonequilibrium molecular dynamics simulations, Nano Lett. 11 (2011) 3917–3921.
[23] N. Khosravian, M.K. Samani, G.C. Loh, G.C.K. Chen, D. Baillargeat, B.K. Tay, Effects of a grain boundary loop on the thermal conductivity of graphene: a molecular dynamics study, Comput. Mater. Sci. 79 (2013) 132–135.
[24] Y.Y. Zhang, Y. Cheng, Q.P. Pei, C.M. Wang, Y. Xiang, Thermal conductivity of defective graphene, Phys. Lett. A 376 (2012) 3668–3672.
[25] H. Malekpour, P. Ramnani, S. Srinivasan, G. Balasubramanian, D.L. Nika, A. Mulchandani, Thermal Conductivity of Suspended Graphene with Defects, 2016 arXiv:1603.05286.
[26] X. Zhang, Y. Gao, Y. Chen, M. Hu, Robustly engineering thermal conductivity of bilayer graphene by interlayer bonding, Sci. Rep. 6 (2016) 22011–22023.
[27] M.T. Pettes, I. Jo, Z. Yao, L. Shi, Influence of polymeric residue on the thermal conductivity of suspended bilayer graphene, Nano Lett. 11 (2011) 1195–1200.

[28] W. Regan, N. Alem, B. Alemán, B. Geng, C. Girit, L. Maserati, et al., A direct transfer of layer-area graphene, Appl. Phys. Lett. 96 (2010) 113102–113105.
[29] S. Plimpton, Fast parallel algorithms for short-range molecular dynamics, J. Comput. Phys. 117 (1995) 1–19.
[30] S. Plimpton A. Thompson and P. Crozier, LAMMPS Molecular Dynamics Simulator.
[31] G. Barbarino, C. Melis, L. Colombo, Effect of hydrogenation on graphene thermal transport, Carbon 80 (2014) 167–173.
[32] G. Barbarino, C. Melis, L. Colombo, Intrinsic thermal conductivity in monolayer graphene is ultimately upper limited: a direct estimation by atomistic simulations, Phys. Rev. B 91 (2015) 035416–035420.
[33] K.R. Hahn, C. Melis, L. Colombo, Structural, vibrational, and thermal properties of nanocrystalline graphene in atomistic simulations, J. Phys. Chem. C 120 (2016) 3026–3035.
[34] C. Melis, L. Colombo, Lattice thermal conductivity of $Si_{1-x}Ge_x$ nanocomposites, Phys. Rev. Lett. 112 (2014) 065901–065906.
[35] E. Lampin, P.L. Palla, P.-A. Francioso, F. Cleri, Thermal conductivity from approach-to-equilibrium molecular dynamics, J. Appl. Phys. 114 (2013) 033525–033530.
[36] H. Zhou, W.J. Yu, L. Liu, R. Cheng, Y. Chen, X. Huang, et al., Chemical vapour deposition growth of large single crystals of monolayer and bilayer graphene, Nat. Commun. 4 (2013) 2096.
[37] I. Vlassiouk, M. Regmi, P. Fulvio, S. Dai, P. Datskos, G. Eres, et al., Role of hydrogen in chemical vapor deposition growth of large single-crystal graphene, ACS Nano 7 (2011) 6069–6076.
[38] A. Eckmann, A. Felten, A. Mishchenko, L. Britnell, R. Krupke, K.S. Novoselov, et al., Probing the nature of defects in graphene by Raman spectroscopy, Nano Lett. 12 (2012) 3925–3930.
[39] A.C. Ferrari, J. Robertson, Interpretation of Raman spectra of disordered and amorphous carbon, Phys. Rev. B 61 (2000) 14095–14107.
[40] A.C. Ferrari, D.M. Basko, Raman spectroscopy as a versatile tool for studying the properties of graphene, Nat. Nanotechnol 8 (2013) 235–246.
[41] I. Calizo, A.A. Balandin, W. Bao, F. Miao, C.N. Lau, Temperature dependence of the Raman spectra of graphene and graphene multilayers, Nano Lett. 9 (2007) 2645–2649.
[42] I. Chatzakis, H. Yan, D. Song, S. Berciaud, T.F. Heinz, Temperature dependence of the anharmonic decay of optical phonons in carbon nanotubes and graphite, Phys. Rev. B 83 (2011) 205411–205416.
[43] A.I. Cocemasov, D.L. Nika, A.A. Balandin, Phonons in twisted bilayer graphene, Phys. Rev. B 88 (2013) 035428–035440.
[44] A.A. Balandin, Thermal properties of graphene and nanostructured carbon materials, Nat. Mater. 10 (2011) 569–581.
[45] Y. Lu, J. Guo, Thermal transport in grain boundary of graphene by non-equilibrium Green's function approach, Appl. Phys. Lett. 101 (2012) 043112–043117.
[46] A.Y. Serov, Z.-Y. Ong, E. Pop, Effect of grain boundaries on thermal transport in graphene, Appl. Phys. Lett. 102 (2013) 033104–033109.
[47] S. Ghosh, W. Bao, D.L. Nika, S. Subrina, E.P. Pokatilov, C.N. Lau, et al., Dimensional crossover of thermal transport in few-layer graphene materials, Nat. Mater 9 (2010) 555–558.
[48] L. Lindsay, D.A. Broido, N. Mingo, Fluxural phonons and thermal transport in multilayer graphene and graphite, Phys. Rev. B 23 (2011) 235428–235433.
[49] D. Singh, J.Y. Murthi, T.S. Fisher, Mechanism of thermal conductivity reduction in few-layer graphene, J. Appl. Phys. 110 (2011) 044317–044325.
[50] E.E. Helgee, A. Isacsson, Scattering of flexural acoustic phonons at grain boundaries in graphene, Phys. Rev. B 90 (2014) 045416–045426.
[51] J.-W. Jiang, B.-S. Wang, J.-S. Wang, H.S. Park, A review on the flexural mode of graphene: lattice dynamics, thermal conduction, thermal expansion, elasticity and nanomechanical resonance, J. Phys. Condens. Matter 27 (2015) 083001–083025.